GOSAT-2 TANSO-FTS-2 SWIR L2 Version 02 Products

Yukio Yoshida*[1], Yu Someya[1], Hirofumi Ohyama[1], Hiroshi Suto[2], Isamu Morino[1], Tsuneo Matsunaga[1], and TCCON partners[3]
1. National Institute for Environmental Studies, Japan, 2. Japan Aerospace Exploration Agency, Japan, 3. https://tccon-wiki.caltech.edu/

I will be at my poster during the following times.
July 12 : 13:30 ~ 15:00, 18:00 ~ 19:00 JST
July 13 : 10:00 ~ 12:00, 13:30 ~ 15:00 JST

GOSAT-2 Product is available via following web site.
SWIR L2 V02.00 will be released to General Users in Early August.
https://prdct.gosat-2.nies.go.jp/

IWGGMS-18
18TH INTERNATIONAL WORKSHOP ON GREENHOUSE GAS MEASUREMENTS FROM SPACE

1. GOSAT-2 / TANSO-FTS-2

The Greenhouse gases Observing SATellite-2 (GOSAT-2), the successor to the GOSAT (2009 - current), was launched on 29 October 2018, and its operational observation has started from February 2019. GOSAT-2 is equipped with two instruments: the Thermal And Near-infrared Sensor for carbon Observation Fourier Transform Spectrometer-2 (TANSO-FTS-2) (Table 1) and the Carbon and Aerosol Imager-2 (TANSO-CAI-2). TANSO-CAI-2 can detect optically thick clouds within the TANSO-FTS-2 instantaneous field-of-view (IFOV).

TANSO-FTS-2 observation is performed at the observation points divided one orbit into 1246 (n = 0, 1, 2, ..., 1245) with interval of about 4.67 seconds (Fig. 1). A unique serial number in one orbit the sounding ID, is attached to each sounding from one ascending node to the next ascending node. The sounding ID corresponds argument of latitude of satellite, and roughly corresponds the latitude of the observation target.

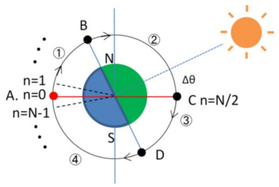

Fig. 1 Schematic of sounding ID.

Table 1. Specifications of TANSO-FTS-2

	Band 1	Band 2	Band 3	Band 4	Band 5
Polarization observation	Yes	Yes	Yes	No	No
Spectral coverage [cm^{-1}]	12950 ~ 13250	5900 ~ 6400	4200 ~ 5200	1188 ~ 1800	700 ~ 1188
FWHM of the instrument line shape function	< 0.4 cm^{-1}	< 0.27 cm^{-1}	< 0.27 cm^{-1}	< 0.27 cm^{-1}	< 0.27 cm^{-1}
Sampling step	< 0.2 cm^{-1}	< 0.2 cm^{-1}	< 0.2 cm^{-1}	< 0.2 cm^{-1}	< 0.2 cm^{-1}
Interval time of data acquisition	Approx. 4.67 sec. (Time required for interferogram acquisition: 4.024 sec.)				
IFOV	15.8 mrad (Diameter projected on the earth's surface at the nadir point of the satellite: approx. 9.7 km)				
FOV	±40° (Along track direction), ±35° (Cross track direction)				

2. TANSO-FTS-2 SWIR L2 column-averaged dry-aur mole fraction product

The column-averaged dry air mole fractions of carbon dioxide, methane, carbon monoxide, and water vapor (XCO_2, XCH_4, XCO, and XH_2O; hereinafter called Xgas), retrieved from Short-Wavelength InfraRed (SWIR) spectral data (Bands 1, 2, and 3 at 0.75–0.77, 1.56–1.69, and 1.92–2.33 μm, respectively) using a so-called full-physics retrieval method, are released as the "GOSAT-2 TANSO-FTS-2 SWIR L2 Column-averaged Dry-air Mole Faction Product" (hereinafter called SWFP).

Retrieval uncertainties of Xgas are evaluated primarily by comparing with the Total Carbon Column Observing Network (TCCON) data. GOSAT-2 SWFP V01.07 shows relatively lower precision of Xgas (Fig. 2) than GOSAT SWIR L2 V02.9x (1.73 ppm for XCO_2 and 0.010 ppm for XCH_4; figure not shown). The mean squared of the residual spectrum (MRS) also shows relatively wide scatter, and an unexpected sinusoidal-shaped large MRS belt can be seen (Fig. 3) This sinusoidal pattern indicates that the root cause of large MRS is not the characteristics of the observed target but the characteristics of TANSO-FTS-2.

3. Analysis of the on-orbit calibration data

To evaluate the characteristics of TANSO-FTS-2, on-orbit calibration data is investigated.

The instrumental line shape function (ILSF) calibration is performed using two types of diode laser (0.77 and 1.54 μm) diffused via an integrating sphere to illuminate the full field of view of the interferometer. From the observed spectrum, the maximum value and its position as well as the full-width at half maximum (FWHM) are derived (Figs. 4 and 5). The maximum value and its position seem to depend on the temperature of the interferometer. On the other hand, FWHM shows less temperature dependence and slightly scattered (0.2 ~ 0.3%), although the laser temperature are stable enough. Also, Band 1 FWHM gradually increases with time. The ILSF used in the SWIR L2 retrieval are time invariant, therefore these behavior might be the reason for the large MRS and retrieval error.

Furthermore, ILSF calibration data shows weak ghost signals on each side of the parent monochromatic line (Fig. 6). Such ghost signals appeared only in Band 1 for GOSAT, but appear in both Band 1 and 2 for GOSAT-2. The ghost signals seem to bring additional retrieval error.

Regarding the sinusoidal pattern shown in Fig. 3, typical temperatures obtained at various satellite locations and their differences between two consecutive soundings show similar patterns (Fig. 7). There seems to be some time lag, but it seems that there is a relationship between temperature and retrieval error.

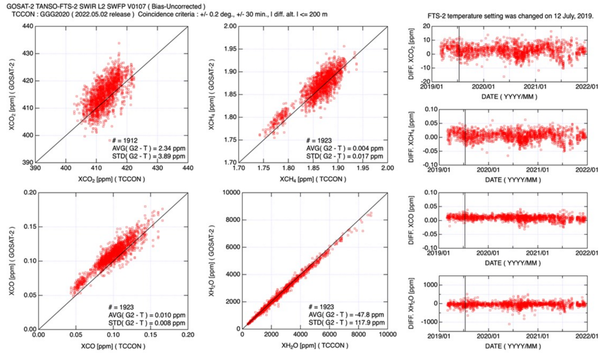

Fig. 2 Comparison between SWFP (V01.07) and TCCON (GGG2020).

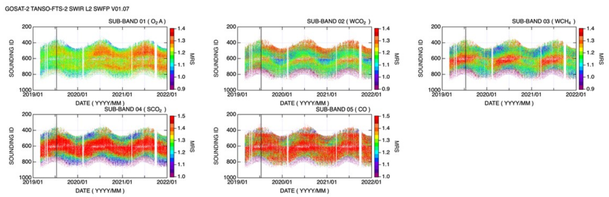

Fig. 3 Time series of the mean squared of the residual spectrum (MRS) for SWFP V01.07.

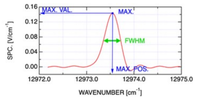

Fig. 4 Schematics of the spectrum obtained ILSF calibration.

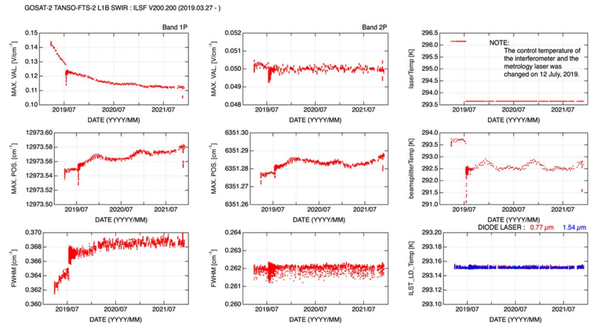

Fig. 5 Time series of the maximum value, its position, and FWHM of ILSF calibration.

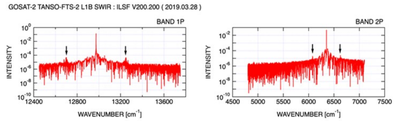

Fig. 6 Example of ghost signals seen in the ILSF spectra.

4. SWIR L2 V02.00 retrieval algorithm

To suppress the retrieval error due to the change of the FWHM of ILSF and ghost signal, ILS stretch factor and zero-level offset for each sub-band are introduced to the state vector of the SWIR L2 V02.00 retrieval. The ILS stretch factor is a factor for changing the wavenumber step of the ILSF data with the same wavenumber step size. The zero-level offset is a wavenumber-independent radiance offset. Some threshold value for the post-screening is revised, because the MRS of the V02.00 retrieval algorithm becomes much smaller (Fig. 8 top). The simultaneously retrieved ILS stretch factor have sinusoidal pattern as expected (Fig. 8 middle and bottom). This suggests that the ILSF changes each sounding in orbit due to the temperature change of the interferometer. On the other hand, the retrieved zero-level offset depends on the intensity of the input radiance. Relatively large zero-level offset values around sounding IDs between 500 and 600 correspond to observations over Sahara Desert.

By introducing these parameters, the standard deviation of the difference between retrieved Xgas and TCCON Xgas is reduced (Fig. 9 red square). Seasonal cycle shown in Xgas differences for SWFP V01.07 has also been reduced. By applying an empirical bias correction based on the multivariate linear regression, both bias and scatter are further reduced (Fig. 9 blue cross). One thing to note is that the ILS stretch factors show a small positive slope with respect to Xgas differences, i.e., ILS stretch factors less than unity corresponds narrower ILSF and tends to show a negative bias in Xgas. This tendency indicates that the ILSF treatment in the retrieval must be further improved to represent the actual ILSF changes in orbit.

NOTE : Research ID "RCFG2083" has the same retrieval settings as the SWIR L2 V02.00 retrieval but was processed by different computer. Bias correction is still tentative version.

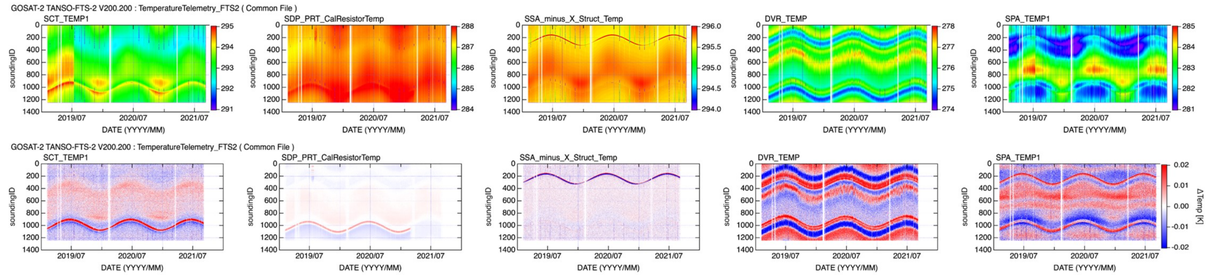

Fig. 7 Time series of typical temperatures obtained at various satellite locations (upper panel) and their differences between two consecutive soundings (lower panel).

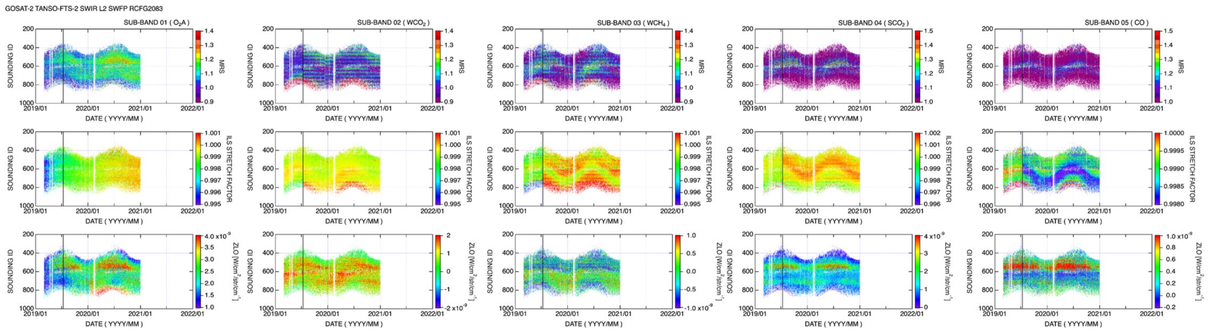

Fig. 8 Time series of MRS, retrieved ILS stretch factor, and retrieved zero-level offset (ZLO).

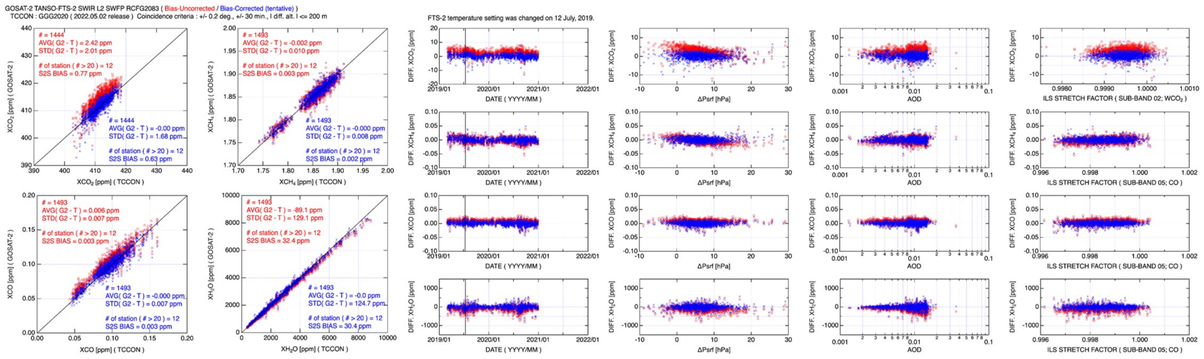

Fig. 9 Comparison between V02.00 retrieval results and TCCON.